OPEN ACCESS Freely available online

Journal of Aeronautics & Aerospace Engineering

Research Article

Study of Magnus Effect Using Rotating Cylinder on Airfoil at Different Locations

Dharmendra P[1], Pavithra Sullad[2], Niharika Mallapur[2*]

[1]*Department of Aeronautical engineering, KLS Gogte institute of Technology, Karnataka, India*

[2] *Department of Aeronautical engineering, KLS Gogte institute of Technology, Karnataka, India*

ABSTRACT

The need for improving the aerodynamic efficiency and delaying the formation of stall over the wing has been of concern in the realm of aviation. The main intention of the project is to improve these two parameters. The configuration used for analysis consists of a NACA (National advisory committee for aeronautics) 2412 airfoil of chord length 0.982m with a cylinder of 0.064m diameter at 0.15c (chord), 0.3c, and 0.45c as our models. The models were designed in SOLIDWORKS and analysis is executed using ANSYS Fluent. The turbulence model used is Spalart Allmaras with a freestream velocity of 10m/s and the RPM of the cylinders is -25000 (clockwise). The influence of various parameters like horizontal and vertical distances from the leading edge and chord line is investigated. The rotating cylinder configurations are compared with the bare airfoil's aerodynamic characteristics, pressure and velocity contours.

Keywords: Magnus effect; Rotating cylinder; Coefficient of lift; Coefficient of drag; Aerodynamic efficiency; Validation; contours

INTRODUCTION

In the field of aeronautics, understanding the flow behaviour over the surface of an airfoil is important. The path to improve the aerodynamic characteristics of the airfoil are provided by this. Not only to design advanced aircrafts but also to control the boundary layer, it is important to delay the boundary layer separation and to improve the lift to drag ratio of the airfoil. The lift generated during flying is one of the most important factors for the flight of an aerial vehicle. The production of lift depends primarily on the nature of free stream air deflection, which is dependent on the airfoil orientation and its curvature. The momentum and the velocity values in the fluid layers along the perpendicular distance from the surface becomes zero as the flow moves along the airfoil surface. This continues till the point where the flow can no longer be attached to the surface of the airfoil, this phenomenon is called flow separation. Creation of vortices and reversed flow are associated with the flow separation that contribute to a drastic drop in the lift and significantly increases in the drag force of the airfoil. Blowing, suction, vortex generation Flapping wing, flying wing and moving surfaces technique are some of the methods to control the boundary layer [1].

Magnus Effect

A rotating body moving through a fluid deviates from its straight path due to the change in pressure in the fluid caused by variation in velocity generated by the body's spin. The Magnus effect is a manifestation of Bernoulli's theorem; fluid pressure reduces at points where the speed of fluid increases. In case of a cylinder in air rotation, some amount of air is dragged along with the cylinder. The airflow is retarded due to the drag on one side of the cylinder whereas it is increased due to the drag on another. Higher pressure on one side where airflow is slower forces the cylinder in a direction of lower pressure region of the opposite side where a relative increase or growth in airflow occurs; this causes a production of lift over the cylinder when it is rotating in a fluid medium. (Fig 1) A ball moving from right to

***Correspondence to:** Niharika Mallapur, Department of Aeronautical engineering, KLS Gogte institute of Technology, Karnataka, India, Tel: 8904807847; E-mail: niharikamallapur10b@gmail.com

Received date: August 31, 2021; **Accepted date:** November 15, 2021; **Published date:** November 25, 2021

Citation: Dharmendra P, Sullad P, Mallapur N (2021) Study of Magnus Effect Using Rotating Cylinder on Airfoil at Different Locations. J Aeronaut Aerospace Eng 10:p67.

left with a clockwise spin and particle behaviour at top end and wake region of the ball are visible [2].

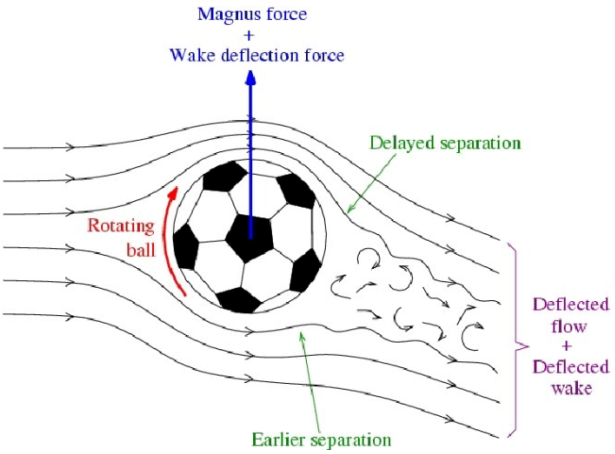

Figure 1: Magnus Effect.

The air moves away from the ball surface creating turbulent spaces just behind the ball to facilitate that the surface of the ball is moving slower relative to the air. The ball's top edge revolves away from the direction of movement. Hence, the stream of air on the side of the ball clings to the surface more and hence is deflected downwards. The force pushing the air down produces an equal and opposite force on the ball upwards, hence confides with Newton's third law; "Every action has an equal and opposite reaction". Perpendicular to the direction of force this force is the Magnus force [3].

A rotating body's deflection is caused by this force in upward direction. A difference in pressure of fluid in opposite sides of the ball can explain the deflection. Magnus effect is caused when a spinning object's body in a fluid creates a perpendicular force called 'lift' and an opposing force called 'drag'. An additional lift force is provided to the airplane by these forces acting on the cylinder. Adjustment of rotating speed of the body varies the drag and lift [4].

The molecules of fluid near an object are disturbed and move around as an object passes through a fluid or as a fluid moves past the object. Thus, aerodynamic forces are generated between the two that is fluid and object. The factors affecting the forces and their magnitude are shape of object, speed of object, and two other important fluid properties that is viscosity and compressibility [5].

The detachment or disconnection of the boundary layer from a surface into a wake region that occurs in flow is known as flow separation or boundary layer separation. Flow against rising pressure is called flowing in adverse pressure gradient. Once it has travelled far enough in adverse pressure gradient the speed of the boundary layer relative to surface has stopped and reversed the direction. The boundary layer in this situation gets separated. The flow takes the forms of eddies and vortices. A constant pressure is exerted by the fluid on the surface instead of a continuous increase in pressure if the layer was still attached. Flow separation causes a reduced lift and increased pressure drag in aerodynamics occurring due to pressure differences between front and rare surfaces of the object. Research and effort towards added features which delay flow separation and keep flow attached for elongated periods as well as much effort has gone into the design of aerodynamic surface contours. The displacement thickness increases sharply of a boundary layer when it separates, which modifies the outside potential flow and pressure field. The pressure field modification in case of airfoil results in increase in drag of pressure and if severe enough will also result in stalls and loses in lift, all undesirable traits. Flow separation produces increased flow loses in terms of internal flows. It also causes stall type phenomena [6].

Momentum injection (Fig 2) enhances the aerodynamic performance of airfoil by keeping the flow attached over top surface of airfoil at a higher angle of attack. Momentum injection by the rotating body helps to delay the flow separation, which acts in an advantageous way for airfoils [7].

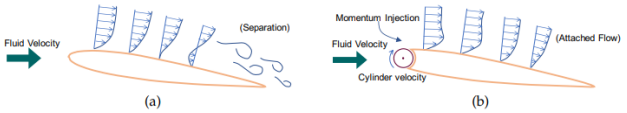

Figure 2: Momentum Injection (a) Without cylinder. (b) With rotating cylinder.

NACA 2412 is the chosen airfoil. It is a type of cambered airfoil and belongs to the four-digit series among the NACA classification of airfoils. The 4-digit, 5-digit and modified 4-/5digit NACA airfoil series were generated based on analytical equations which describe the camber of airfoil section as well as the thickness of airfoil along its length, the two primary variables that affect the shapes of airfoil are the slope of the airfoil mean chamber line and its thickness above and below this line. Series of equation were presented incorporating these two variables which could be used to produce an entire family of related airfoil shapes [8].

According to NACA four-digit series definition, NACA2412 (Fig 3) airfoil has a max camber of 20% located at 40% from the leading edge with a maximum thickness of 12% of the chord.

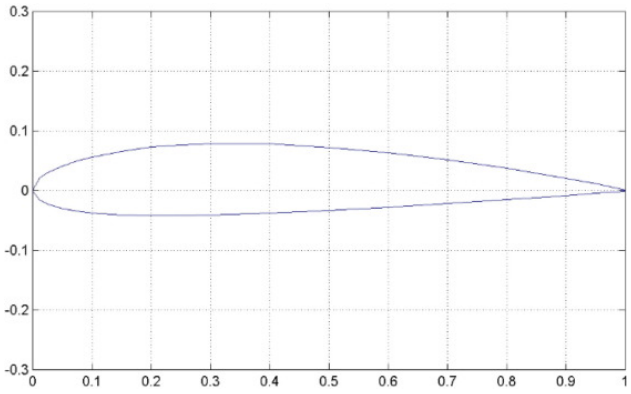

Figure 3: NACA 2412.

Scope of work

- Comprehensive understanding of the boundary layer effects and relatedness with the airfoil body
- To optimize the desirable lift and drag coefficients by designing various cylinder configurations.

- To incur desirable lift and drag by placing the cylinder at different chord locations.
- Finding Acceptable CFD models to improvise the similar topic results.

Objective

- To delay boundary layer separation towards the trailing edge of the airfoil.
- To improve the quality of flow over the airfoil.
- To reduce the exponential increase in Drag at higher angles of attack.
- To increase Critical Angle of attack at which stall occurs.

DESIGN AND METHODOLOGY

Theoretical Background

Magnus effect is the main phenomena that this project revolves around. A rotating cylinder is used in the airfoil at different locations to improve the flow around the airfoil. Thus, there is an increase in the efficiency due to a generation of lift force [9].

Reynolds number (1) is an equation that relates density, viscosity, speed, and size of flow in a non-dimensional equation where fluid dynamics problems are involved. This expression is used in multiple cases related to laminar flow or turbulent flow. Mathematically the Reynolds number of a situation is expressed as the following:

The Reynolds number (Re) for the analysis is calculated using the below formula as represented below

$Re = \rho u/\mu$ (1)

Where,

ρ = Density (kg/m3) = 1.225 kg/m3

μ = Dynamic viscosity (kg/m*s) = 1.7894*10-5 kg/m*s

L = Length (m) = 0.982 m

u = Flow speed (m/s) =10 m/s

Using (1), a calculated value of about 675000 is obtained for Re which is categorized as turbulent flow. The effect of boundary layer on the surface of airfoil due to rotating cylinder was determined by usage of boundary layer equations like Naiver-Stroke's equation for turbulent flow and incompressible flow [10].

Spalart Allamras CFD model is used to obtain good boundary layer interactions and was found suitable for this project. The model involves the solution of one transport equation. Hence the computational effort is lower compared to 2-equation models. It has been extensively validated for external flows and provides good agreement with experimental results in aerospace application. With this model we can reasonably well predict drag and lift in aerodynamic application for small to moderate angle of attack. $Uc/U\infty$ is the ratio of cylinder rotational speed to free stream velocity [11].

Design of Model

NACA2412 coordinate files were imported using Airfoil Tools into SOLID WORKS where the spline was converted into a 2-D surface and then imported to ANSYS Design Modeller. The geometry (Fig 4, 5, 6) was designed with respect to the thickness of the airfoil at the desired chord percentage. Table (1, 2, 3) gives the dimensions of the geometry. ANSYS Design modeller was used to create domain geometry. To design the final model, multiple approaches were employed like the location of cylinder, size of cylinder, distance from leading edge and height from the chord line [12].

Figure 4: Design of rotating cylinder at 0.15c.

Table1: Dimension of rotating cylinder at 0.15c.

Parameter	Dimension
Cut out cylinder (Diameter)(R1)	70mm
Rotating cylinder (Diameter)(R2)	64mm
Fluid Cylinder (Diameter)	68mm
Horizontal Distance from Leading edge	147mm

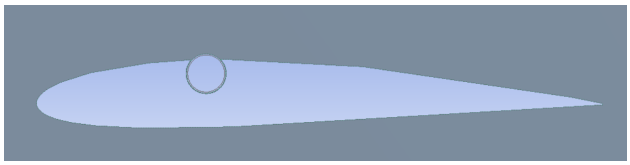

Figure 5: Design of rotating cylinder at 0.30c.

Table2: Dimension of rotating cylinder at 0.30c.

Parameter	Dimension
Cut out cylinder (Diameter)(R1)	70mm
Rotatin cylinder (Diameter)(R2)	64mm
Fluid Cylinder (Diameter)	68mm
Horizontal Distance from Leading edge	294.5mm
Vertical Distance from Chordline	53mm
Chord length	982mm

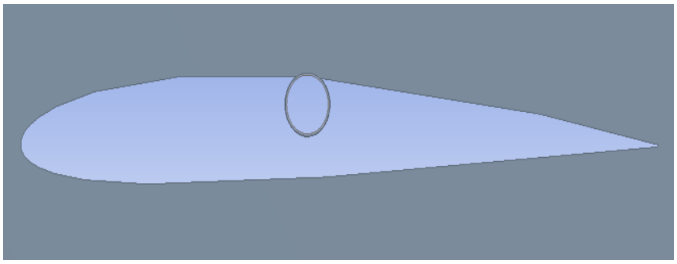

Figure 6: Design of rotating cylinder at 0.45c.

Table3: Dimension of rotating cylinder at 0.45c.

Parameter	Dimension
Cut out cylinder (Diameter)(R1)	70mm
Rotating cylinder (Diameter)(R2)	64mm
Fluid Cylinder (Diameter)	68mm
Horizontal Distance from Leading edge	393mm
Vertical Distance from Chord line	33mm
Chord length	982mm

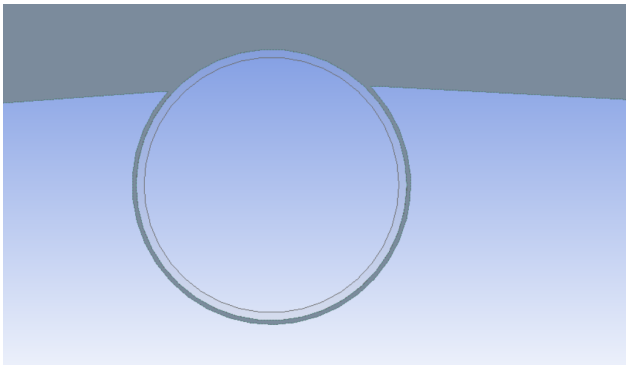

Figure 7: Rotating cylinder.

Design of Domain

The flow domain (Fig 8) size is 6 times the chord length from the leading edge, i.e,6c from the chord line to the far-field, 16c at the outlet from the leading edge which makes sure that there are no far-field interactions. A large domain is demanded so that the flow does not intervene with the walls and accurate results are obtained [13].

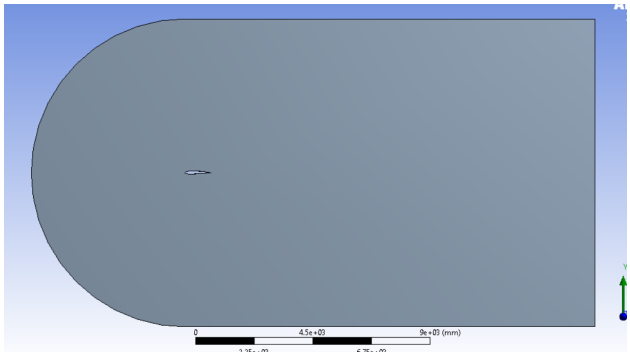

Figure 8: Flow Domain.

Meshing

Standard CFD methods require a mesh that fits the boundaries of the computational domain. The generation of computational mesh that is suitable for the discretized solution of two-dimensional Naiver-Stokes equations has always been the subject of intensive researches [14].

The domain around the airfoil is named as 'Outer fluid'. Since the domain is large and encounters subsonic flow (10m/s), the mesh used is triangular (Fig 9) because it is easy to generate; considering its modest problem statement and area covered by the outer fluid. The domain enveloped around the cylinder is named 'Inner fluid'. The domain is non-linear and is the area of interest. Hence, the quadrilateral mesh is applied (Fig 10). Body sizing and edge sizing is defined with respect to the mesh independency test and to generate dense mesh around the airfoil. The presence of non-linear bodies will cause a contact convergence issue. To evade this condition, Inner fluid, and Outer fluid are bonded using the bonding of surface option. This setting helps to bond across a gap between the surface body in non-linear analysis and giving out more agile solutions.

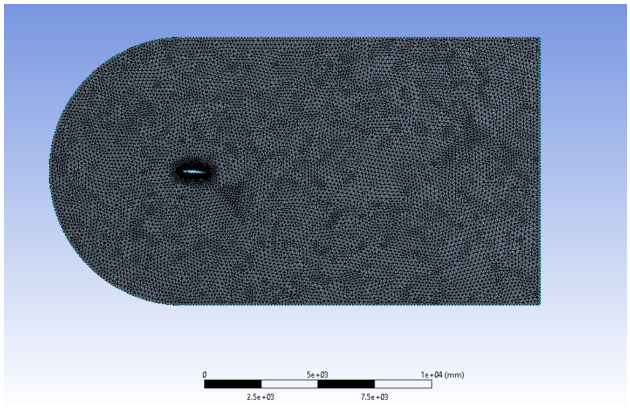

Figure 9: Meshed domain.

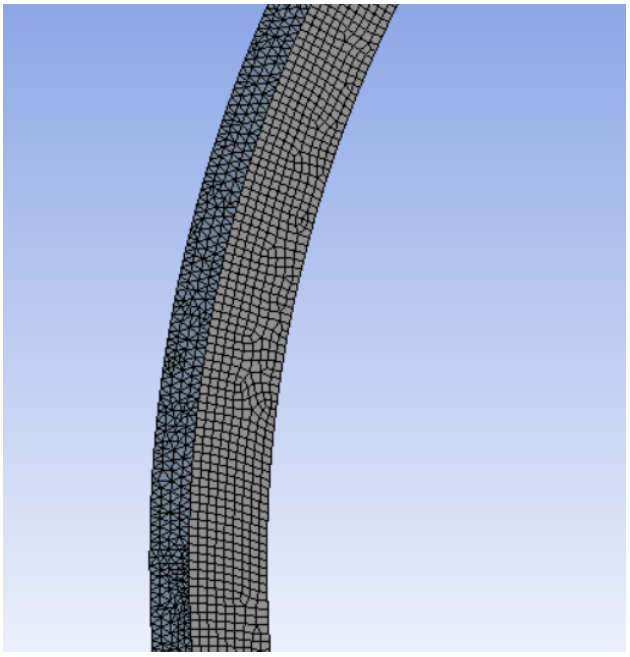

Figure 10: Cylinder meshing.

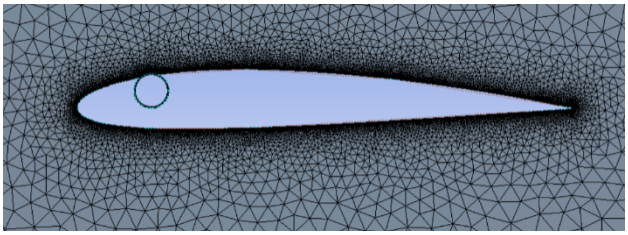

Figure 11: Meshing of 0.15c design.

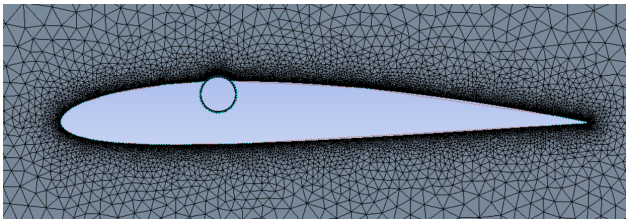

Fig 12: Meshing of 0.30c design.

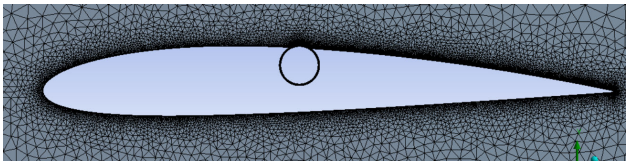

Figure 13: Meshing of 0.45c design.

Mesh Independency Test

This is the way of verifying if the solution is independent of the grid or not to generate a grid with more cells to distinguish the solutions of the two models. (Fig 14) Refining the grid and examining for drag coefficient we find that for about 1200000 cells, the values don't vary substantially affecting the output. This is chosen to improve the accuracy and diminish computation time. *number of elements (105)

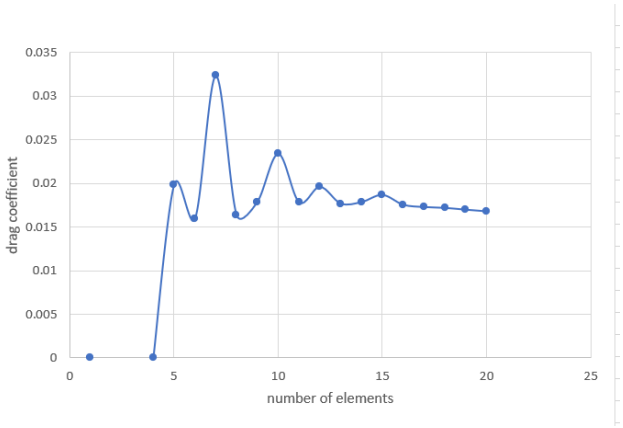

Figure 14: Mesh independency test.

Software Validation

To validate the software, results from the research paper [1]. And obtained results are compared. The error obtained should be within 15% tolerance. This ensures that the results obtained from the software and the methodologies are accurate and positive for the project. (Fig 15) The table (4) gives an insight into the validation that was conducted on the NACA 2412 airfoil.

Table4: Validation results.

Angle of Attack	CL (Reference)	CL (Obtained)	Error %
0	0.204	0.237	16.1
4	0.592	0.617	4.2
8	0.887	0.805	9.2
12	1.103	0.963	12.6
16	1.093	1.104	1

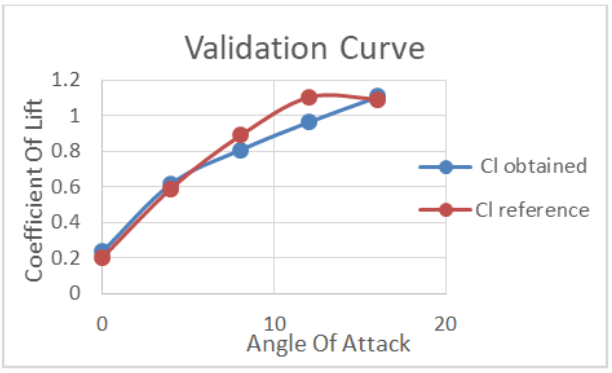

Figure 15: Validation curve.

Setup and Analysis

Spalart-Allmaras Turbulence model was used with moving mesh in cell zone conditions. Inlet velocity used is 10 m/s. The cylinder rotation was varied to an optimal value of about -25000 RPM. The step size was 0.005 to obtain a solution with the

highest accuracy. Lift and Drag coefficients were plotted at airfoil and cylinder location. To maximize the accuracy, the convergence condition was set to 0.001. The reference values were measured from the inlet and hybrid initialization was used. Particle tracking was used to study the flow behaviour around the geometry. The outer fluid and the rotating cylinder were a moving wall boundary condition and the outlet was a pressure outlet with 0-gauge pressure. Max iterations per time step was kept at 30 to obtain results with efficiency. Solution reports of forces were toggled to get real-time values and check for any errors. Additionally, double precision was enabled at the beginning.

RESULTS

Aerodynamics

The following (table 5, 6, 7, 8) are the results obtained after the analysis of three configurations including bare airfoil (Fig 16, 17, 18).

Table5: Results of bare airfoil.

Angle Of Attack	Bare airfoil Cl	Bare airfoil Cd	Cl/Cd
0	0.2372	0.1169	2.06
4	0.6176	0.0182	33.9
8	0.8057	0.0061	134.1
12	0.9632	0.0389	25.34
16	1.1042	0.0607	18.4

With respect to the Table-5 bare

airfoil attains maximum lift coefficient at 16° AoA (Angle of attack) and highest aerodynamic efficiency at 8°.

Cl: Coefficient of lift

Cd: Coefficient of drag

Table6: Results of 0.15c configuration.

Angle Of Attack	0.15c Cl	0.15c Cd	Cl/Cd
0	1.5272	0.0101	152.7
4	3.2523	0.0383	108.3
8	4.3802	0.2234	19.9
12	6.8934	0.3211	21.5
16	8.6788	0.5095	17.3
20	10.447	0.7068	14.91

From Table-6, for rotating cylinder at 0.15c gives higher aerodynamic efficiency at lower angles of attack.

Table7: Results of 0.30c configuration.

Angle Of Attack	0.30c Cl	0.30c Cd	Cl/Cd
0	2.206	0.4949	4.61
4	4.2077	0.4084	10.5
8	6.1001	0.2164	29.04
12	8.3171	0.0836	103.87
16	10.374	0.1794	54.57
20	12.502	0.4292	29.76

As observable from the table-VII it is clear that the rotating cylinder at 0.30c gives highest aerodynamic efficiency at 12° AoA.

Table8: Results of 0.45c configuration.

Angle Of Attack	0.45c Cl	0.45c Cd	Cl/Cd
0	1.2132	0.6978	1.75
4	1.8168	0.762	2.38
8	2.0966	0.6974	3.02
12	2.836	0.7834	3.62
16	3.5278	0.1882	19.55
20	4.0095	0.2852	14.28

From Table-8, for 0.45c configuration higher aerodynamic efficiency showed is at 20° AoA and is it also clear that the performance is moderate compared to other configurations.

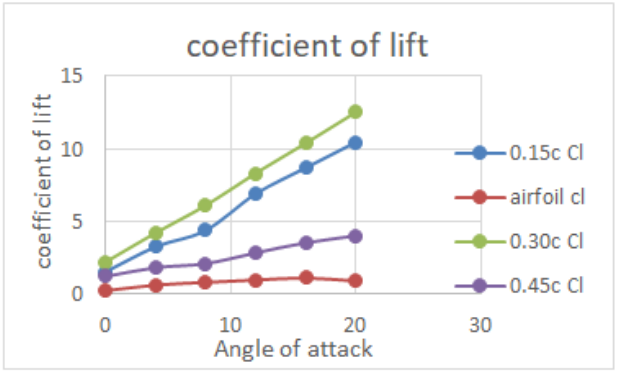

Figure 16: Cl v/s AoA.

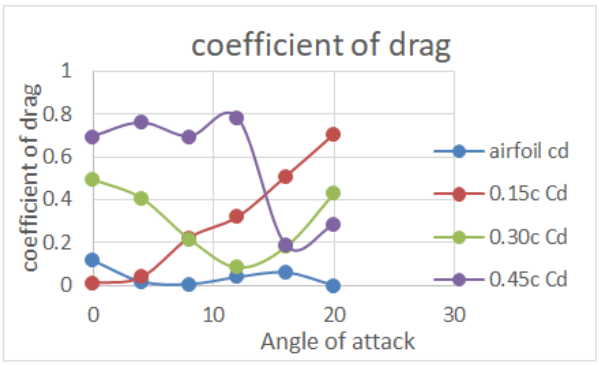

Figure 17: Cd v/s AoA.

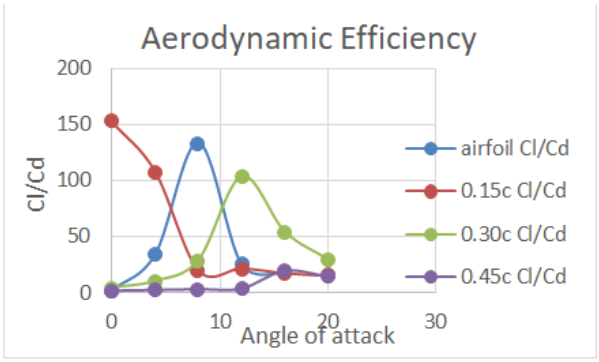

Figure 18: Cl/Cd v/s AoA

(Fig 18) The Bare airfoil has the highest aerodynamic efficiency. However, when comparing the rotating cylinder configurations, it is clear that rotating cylinder configuration of 0.15c at 0° and 4° has the highest aerodynamic efficiency and 0.45c has the least aerodynamic efficiency.

Pressure contours

(Fig 19) The pressure contours are compared between the bare airfoil and the rotating cylinder configuration at an Angle of attack of 0 degree. Looking at the static pressure scale, the pressure has increased in the rotating cylinder configuration.

*The contours are not distinctive due to small variation (inlet velocity 10 m/s). Please refer the scale.

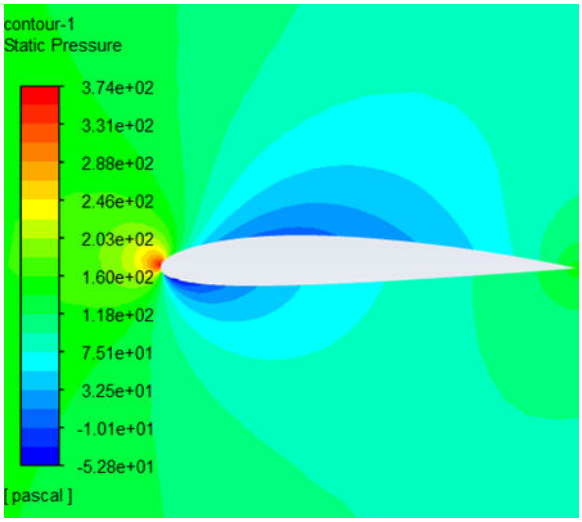

(a)

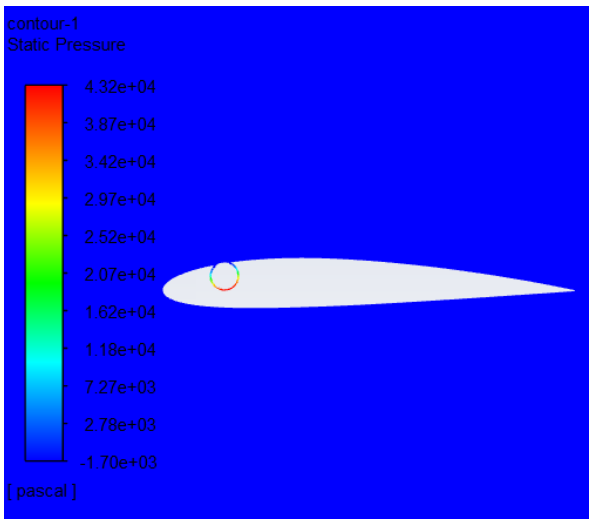

(b)

Figure 19: Pressure contour at 0°. (a) Bare airfoil. (b) 0.15c configuration

(Fig 20) The pressure contours are compared between the airfoil and the rotating cylinder configuration at an Angle of attack of 4°. Looking at the static pressure scale, the pressure has increased in the rotating cylinder configuration due to which lift has also increased.

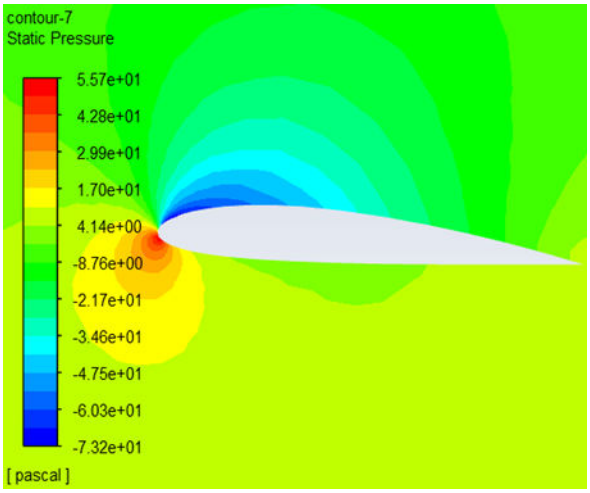

(a)

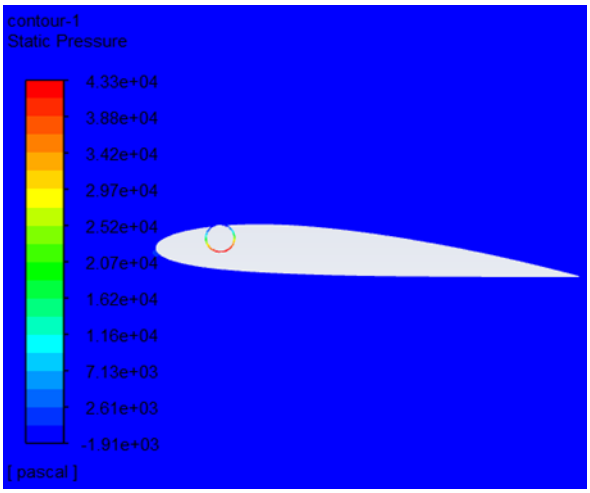

(b)

Figure 20: Pressure contour at 4°; (a) Bare airfoil. (b) 0.15c configuration.

(Fig 21) The pressure contours are compared between the airfoil and the rotating cylinder configuration at an Angle of attack of 8°. There is decrement in static pressure as it can be observed from the suction surface of 0.15c when compared to the previous angle.

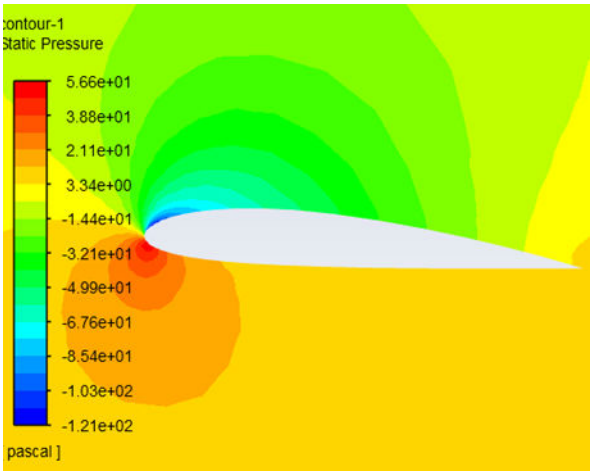

(a)

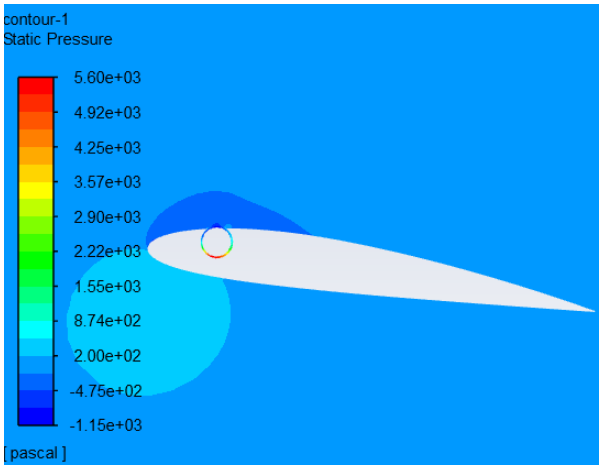

(b)

Figure 21: Pressure contour at 8°; (a) Bare airfoil. (b) 0.15c configuration.

(Fig 22) The pressure contours are compared between the airfoil and the rotating cylinder configuration at an Angle of attack of 12°.

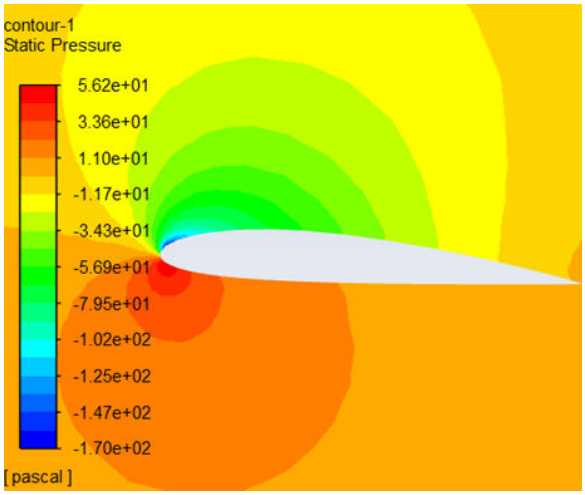

(a)

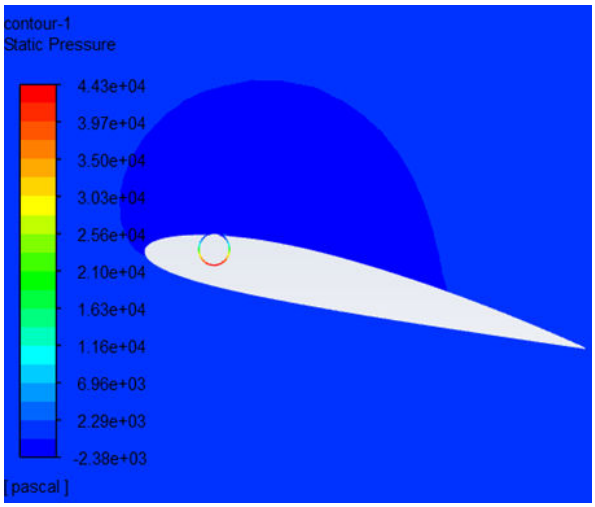

(b)

Figure 22: Pressure contour at 12°; (a) Bare airfoil. (b) 0.15c configuration.

(Fig 23) The pressure contours are compared between the airfoil and the rotating cylinder configuration at an Angle of attack of 16°. In the suction surface of rotating cylinder configuration decrement in pressure is observed with to respect to the previous angle on the same configuration.

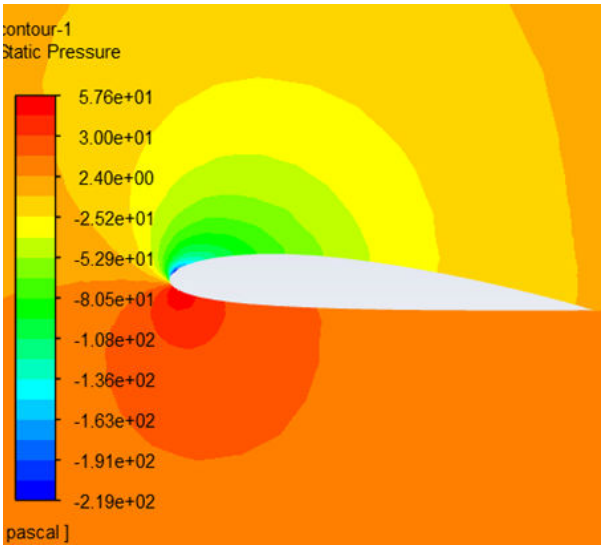

(a)

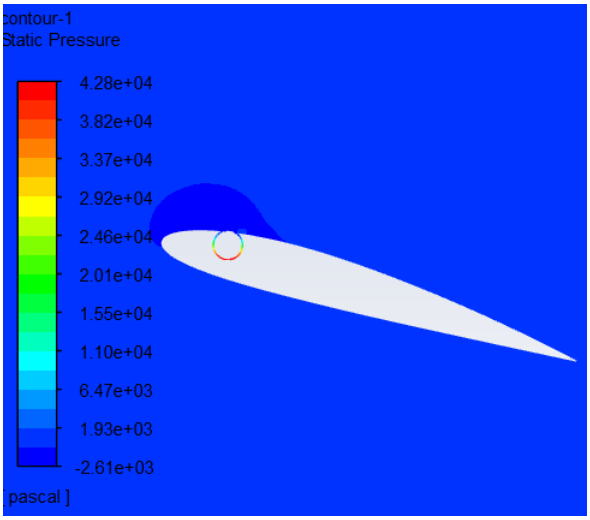

(b)

Figure 23: Pressure contour at 16°; (a) Bare airfoil. (b) 0.15c configuration

(Fig 24) The pressure contours are compared between the airfoil and the rotating cylinder configuration at an Angle of attack of 20°. This configuration at 20° does not show stable aerodynamic configurations when compared with bare airfoil

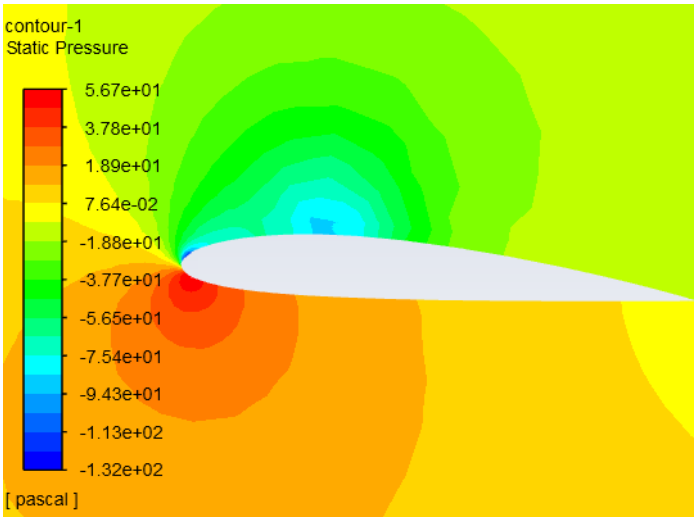

(a)

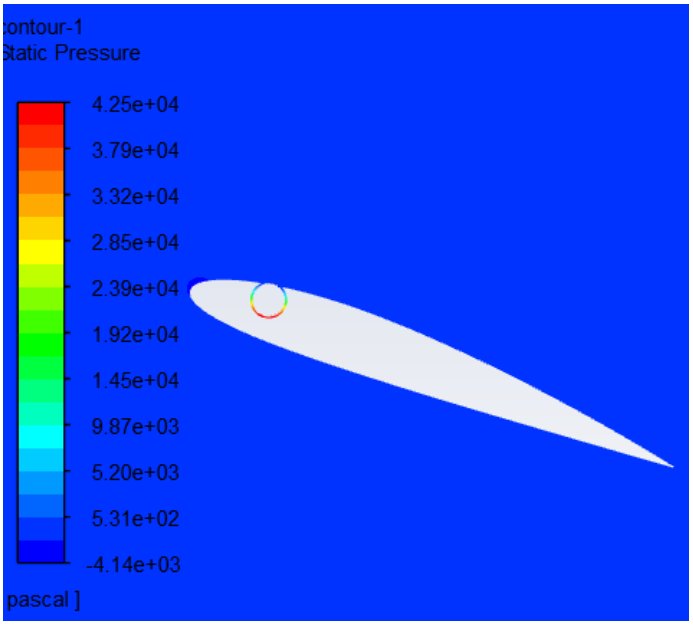

(b)

Figure 24: Pressure contour at 20°; (a) Bare airfoil. (b) 0.15c configuration.

Velocity contours

(Fig 25) The velocity contours are compared between the bare airfoil and the rotating cylinder configuration (0.15c) at an Angle of attack of 0°. The overall velocity has increased in 0.15c configuration when compared to bare airfoil.

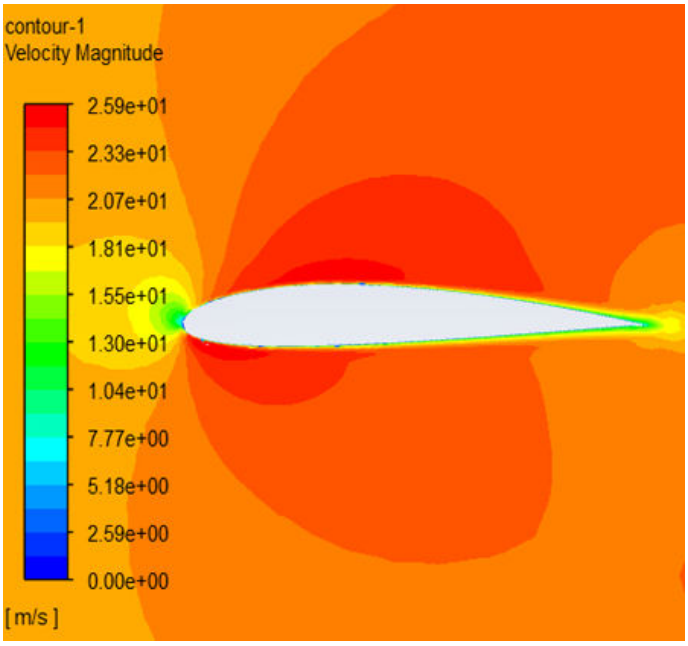

(a)

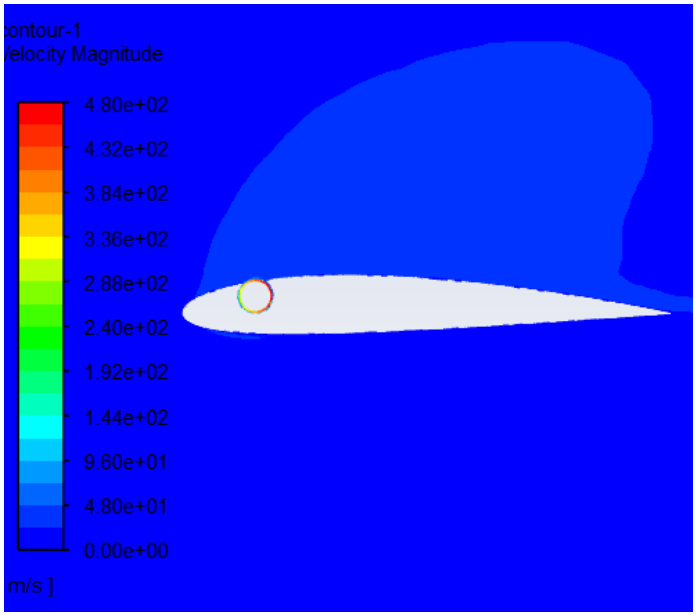

(b)

Figure 25: Velocity contour at 0°; (a) Bare airfoil. (b) 0.15c configuration.

(Fig 26) The velocity contours are compared between the airfoil and the rotating cylinder configuration at an Angle of attack of 4°. As it can be observed on the suction surface of both figures there is huge increment in velocity of 0.15c.

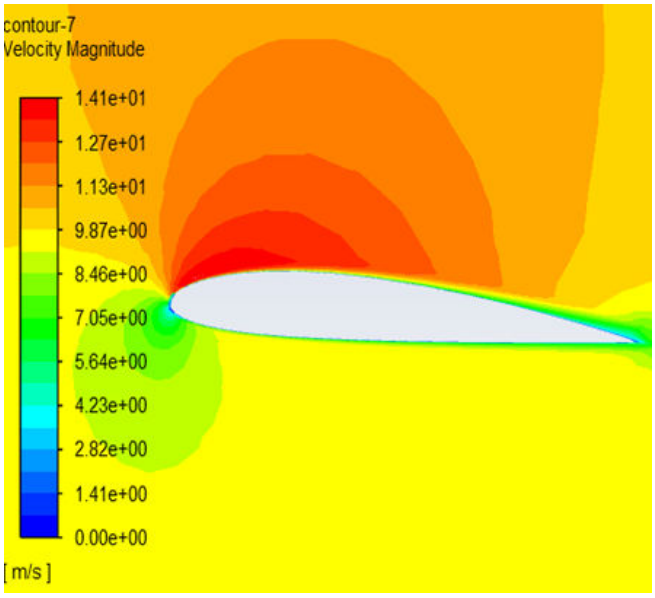

(a)

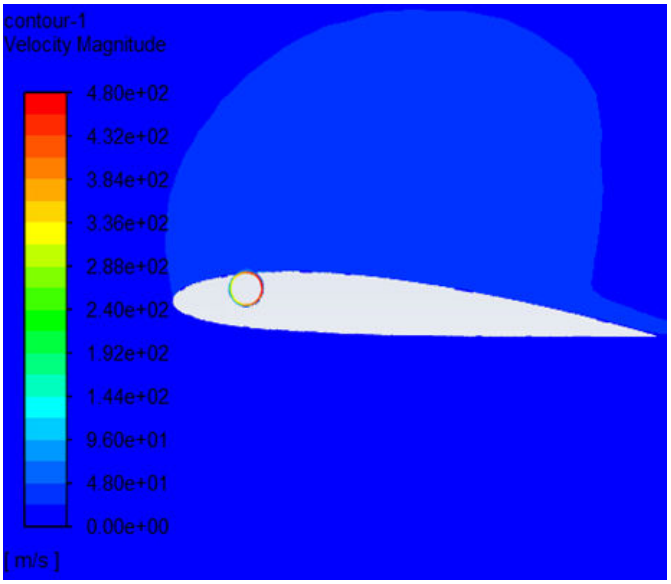

(b)

Figure 26: Velocity contour at 4°; (a) Bare airfoil. (b) 0.15 configuration.

(Fig 27) The velocity contours are compared between the airfoil and the rotating cylinder configuration at an Angle of attack of 8° where it is observed that 0.15c has high velocity on upper surface significantly giving large increase in lift.

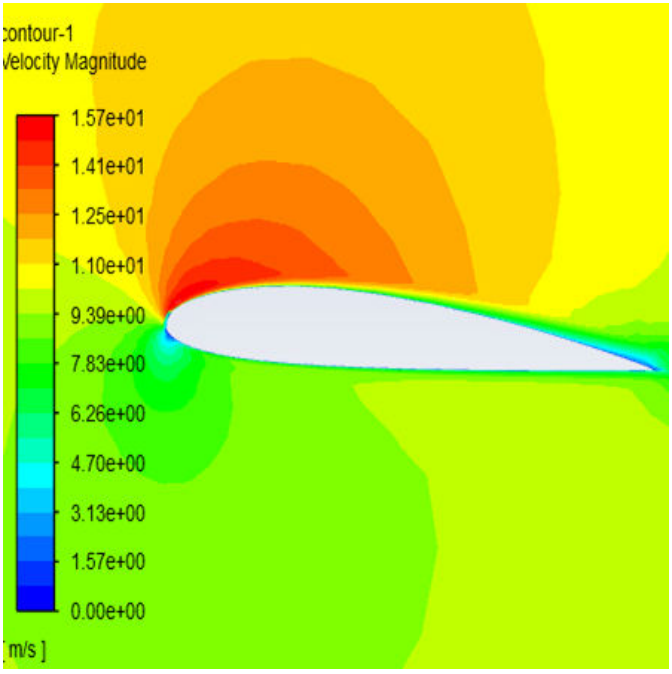

(a)

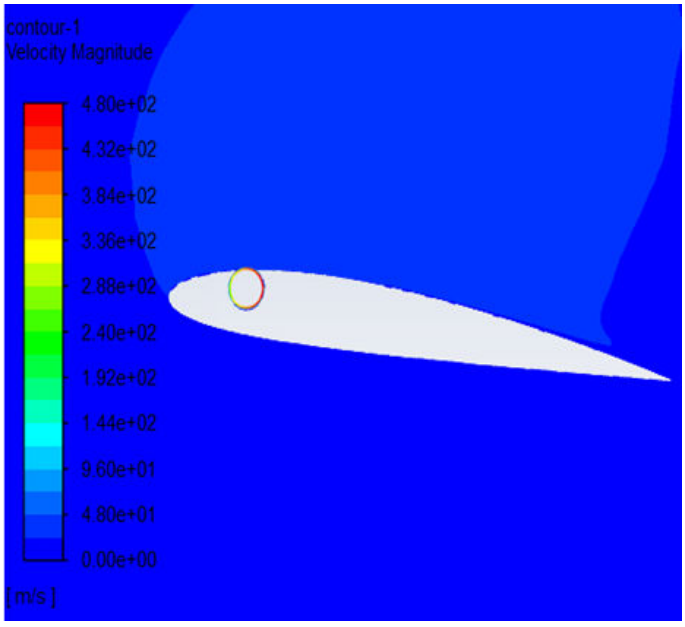

(b)

Figure 27: Velocity contour at 8°; (a) Bare airfoil. (b) 0.15c configuration.

(Fig 28) The velocity contours are compared between the airfoil and the rotating cylinder configuration at an Angle of attack of 12°. As it can be observed on the suction surface of both figures there is huge increment in velocity of 0.15c.

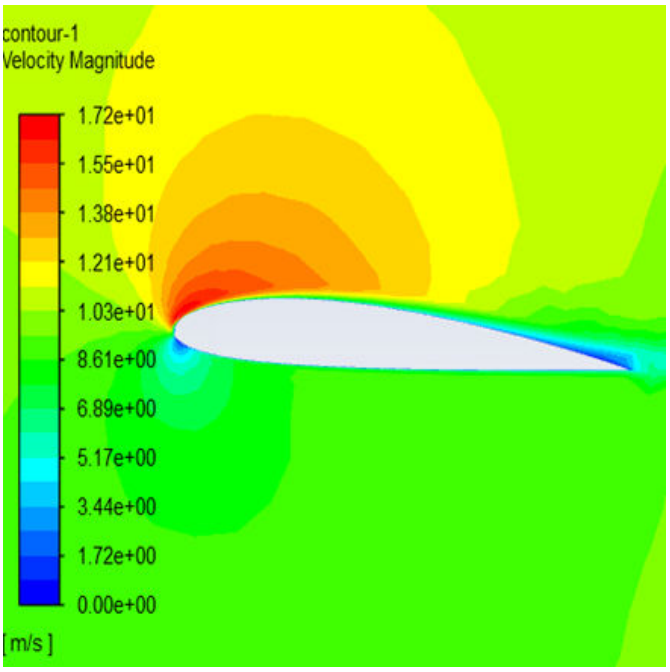

(a)

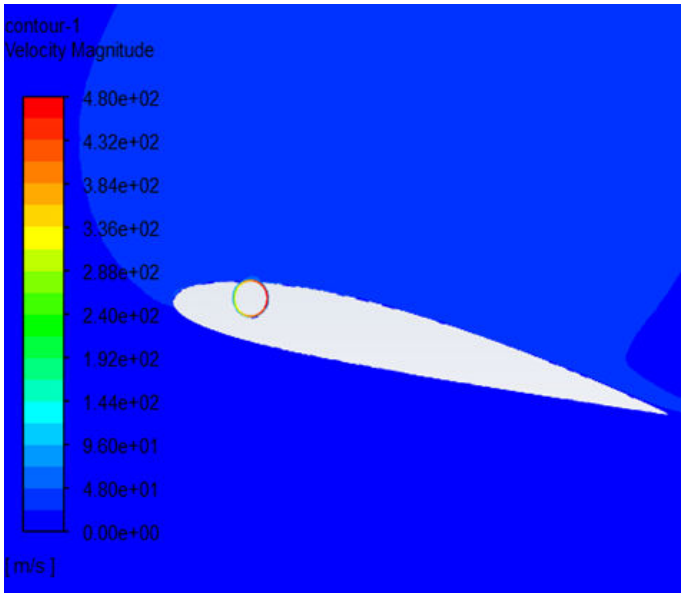

(b)

Figure 28: Velocity contours at 12°; (a) Bare airfoil. (b) 0.15c configuration.

(Fig 29) The velocity contours are compared between the airfoil and the rotating cylinder configuration at an Angle of attack of 16°. The overall velocity has increased in 0.15c configuration when compared to bare airfoil. From the contours it can be said that there is decrement in lift because of early flow separation when compared to previous AoA.

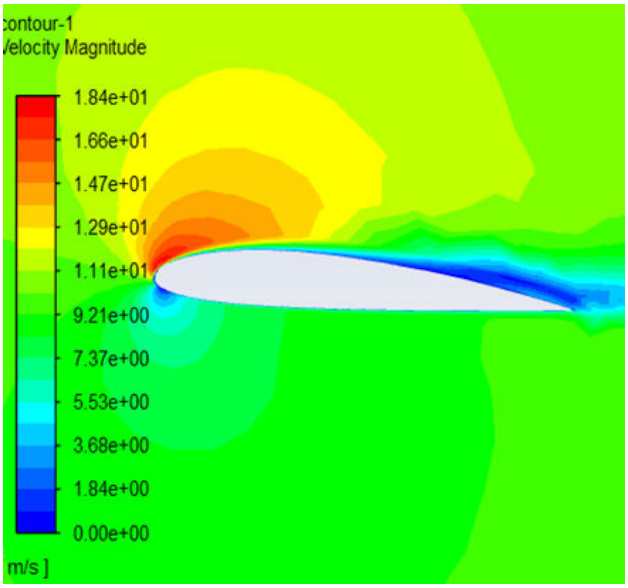

(a)

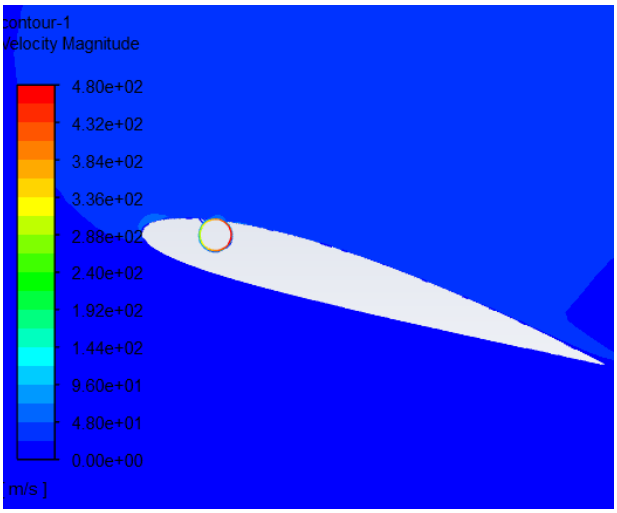

(b)

Figure 29: Velocity contours at 16°; (a) Bare airfoil. (b) 0.15c configuration.

(Fig 30) The velocity contours are compared between the airfoil and the rotating cylinder configuration at a 20 Angle of attack of degree. Again, the early flow separation can be observed in the bare airfoil making decrement in lift coefficient, the same is not true for 0.15c configuration.

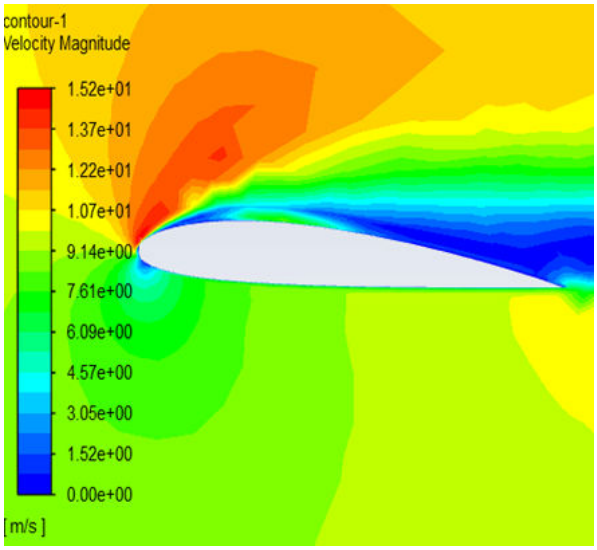

(a)

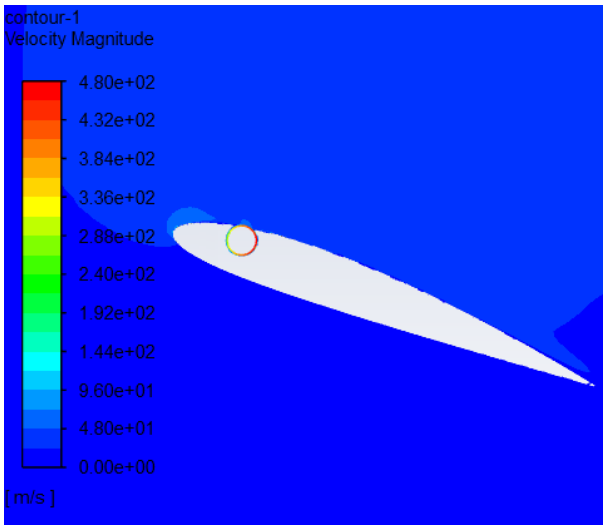

(b)

Figure 30: Velocity Contours; (a) bare air foil. (b) 0.15c configuration.

Contours of 0.30c configuration

Below given contours are the pressure (Fig 31) and velocity contours (Fig 32) for rotating cylinder at 0.30c. It is observed that decrease in pressure accounts for increase in velocity that can be seen in the following figures. Compared to 0.15c and bare airfoil the velocity values are increased hence the lift has huge increment for all the angles of attack.

- Pressure Contour

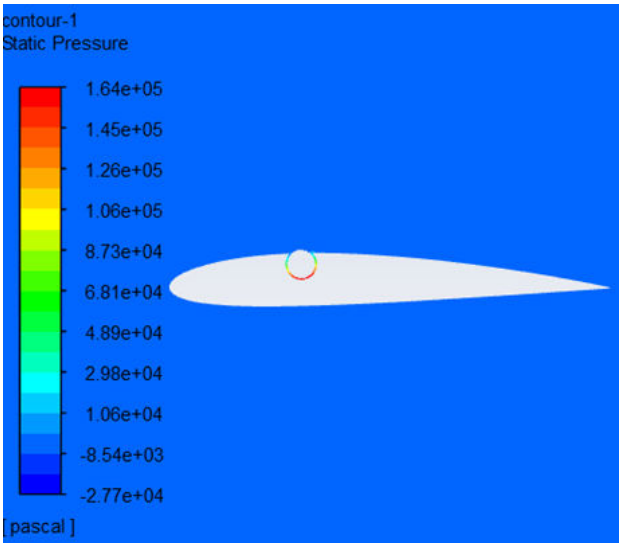

(a)

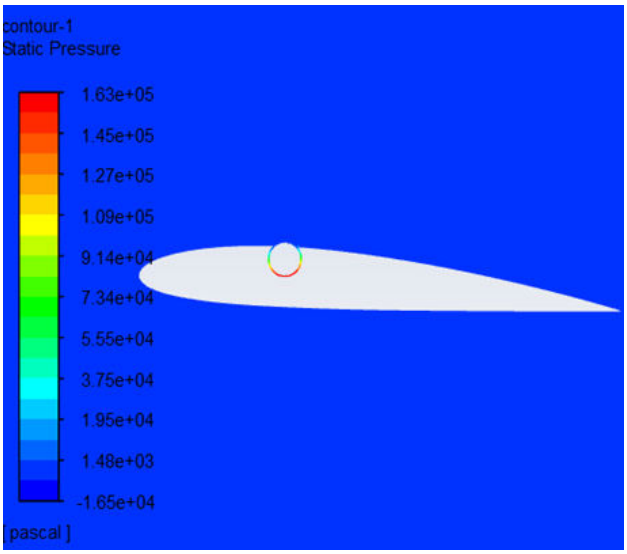

(b)

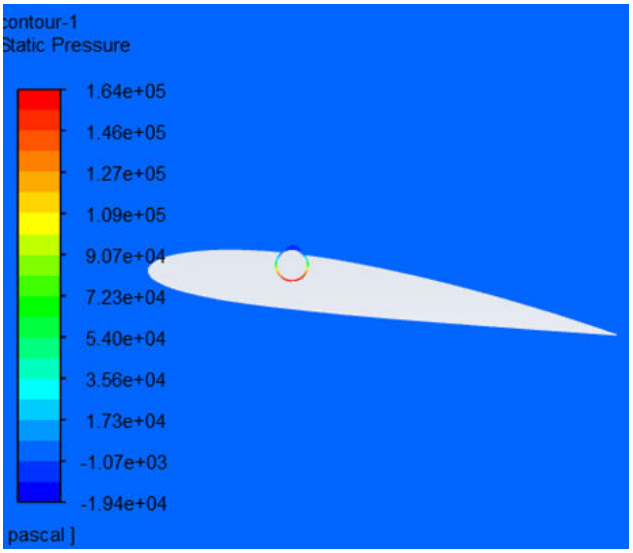

(c)

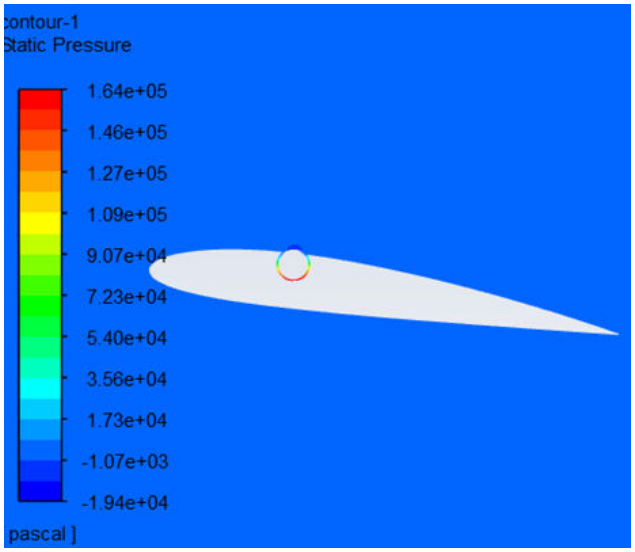

(d)

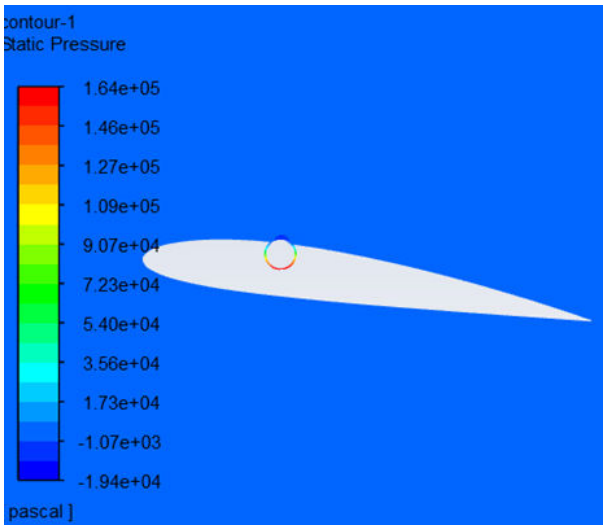

(e)

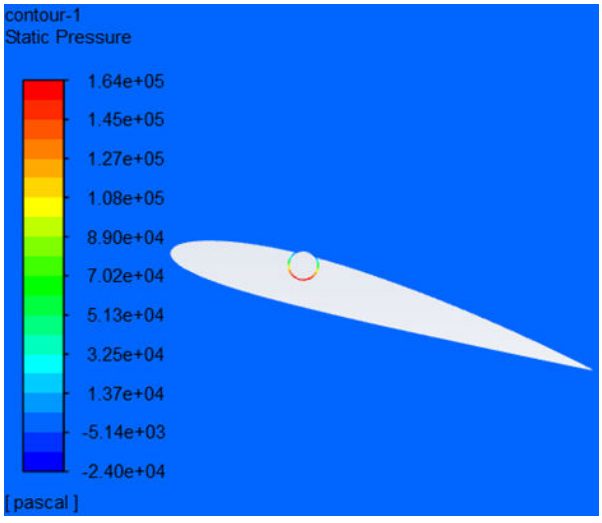

(f)

Figure 31: Pressure contour; (a) At 0°. (b) At 4°. (c) At 8°. (d) At 12°. (e) At 16°. (f) At 20°.

• Velocity contours

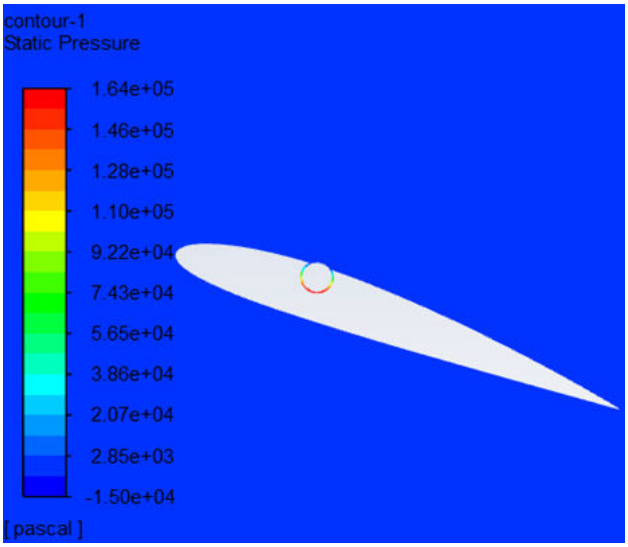

(a)

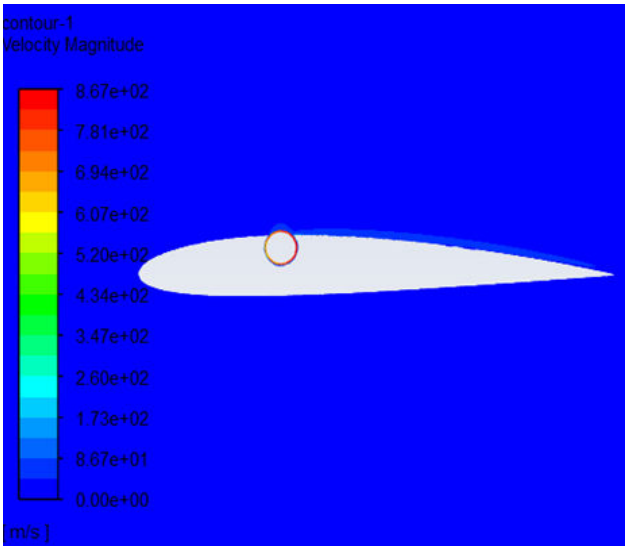

(b)

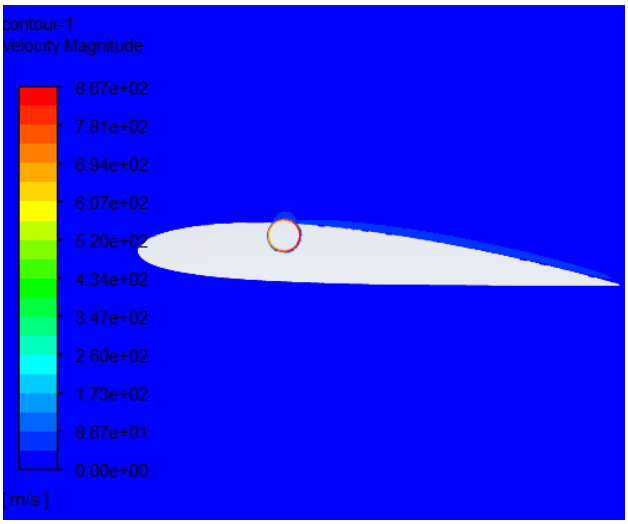

(c)

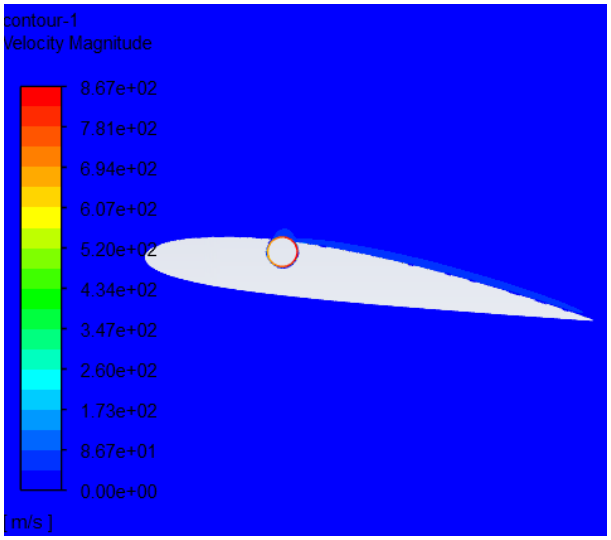

(d)

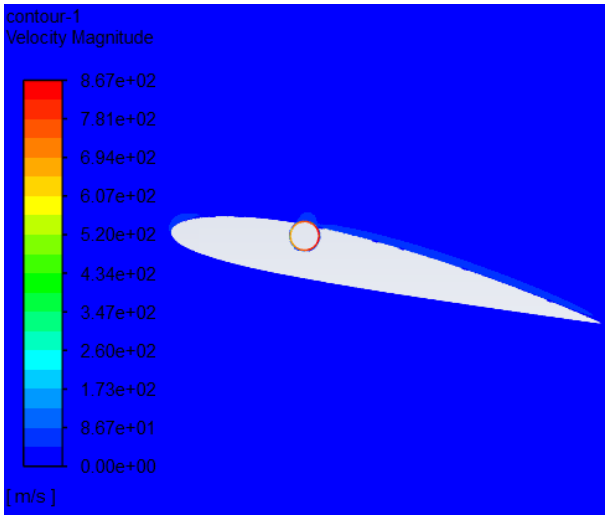

(e)

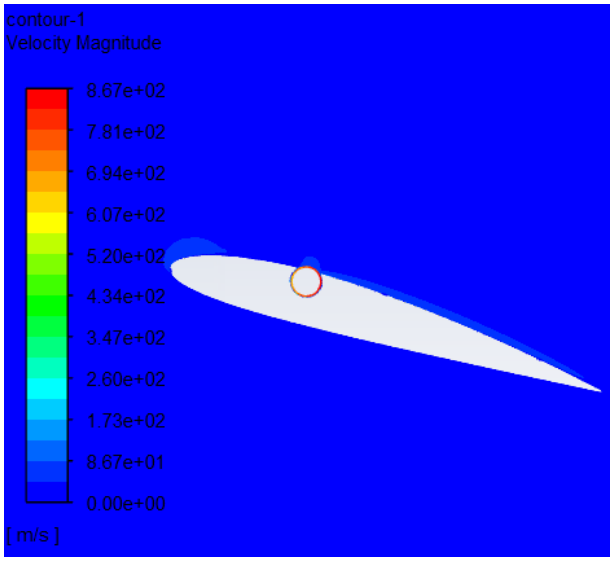

(f)

Figure 32: Velocity contour; (a) At 0°. (b) At 4°. (c) At 8°. (d) At 12°. (e) At 16°. (f) At 20°.

Contours of 0.45c configuration

Below given figures show pressure (Fig 33) and velocity contours (Fig 34) for rotating cylinder at 0.45c. There is negligible difference in pressure and velocity for different angles of attack.

• Pressure contours of 0.45c configuration

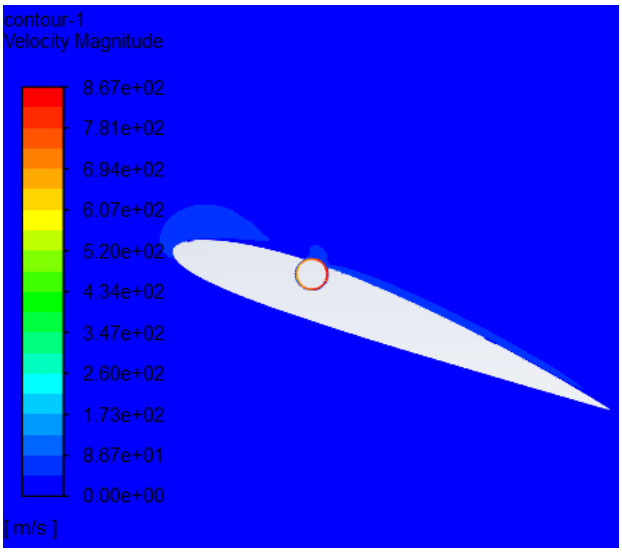

(a)

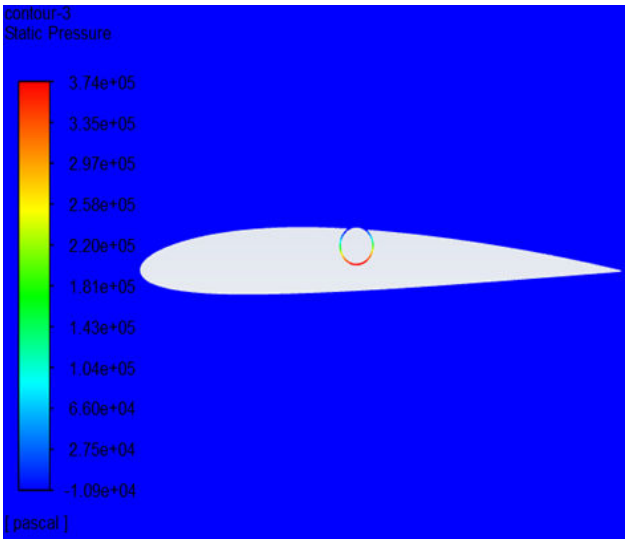

(b)

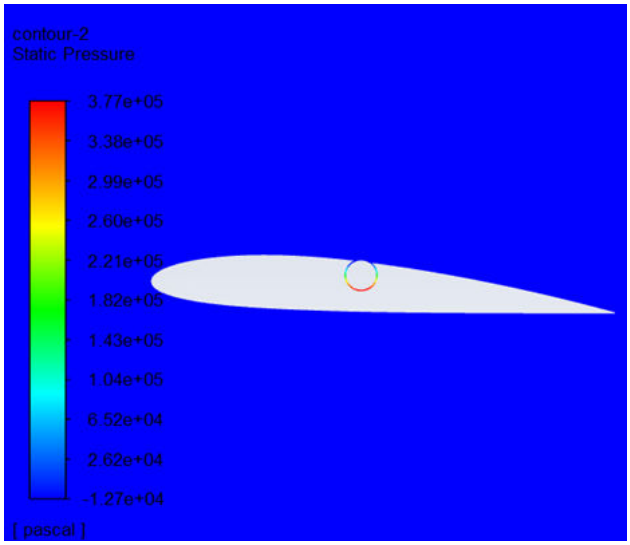

(C)

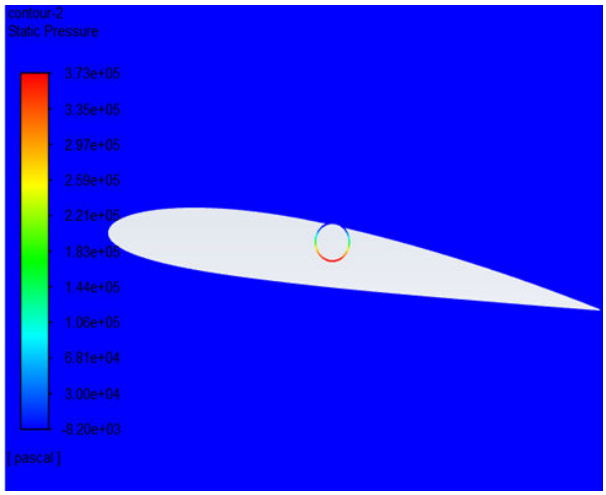

(d)

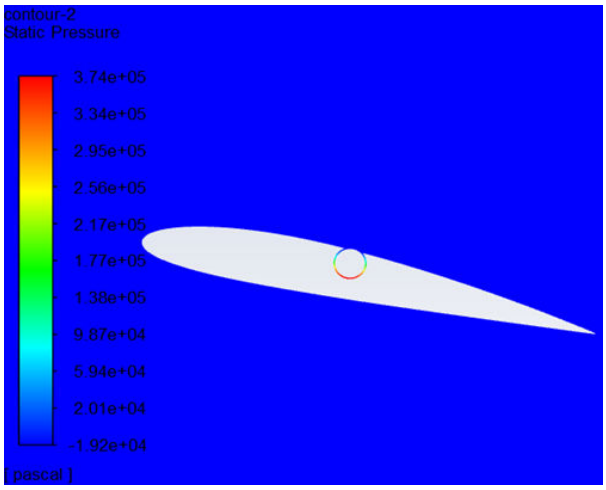

(e)

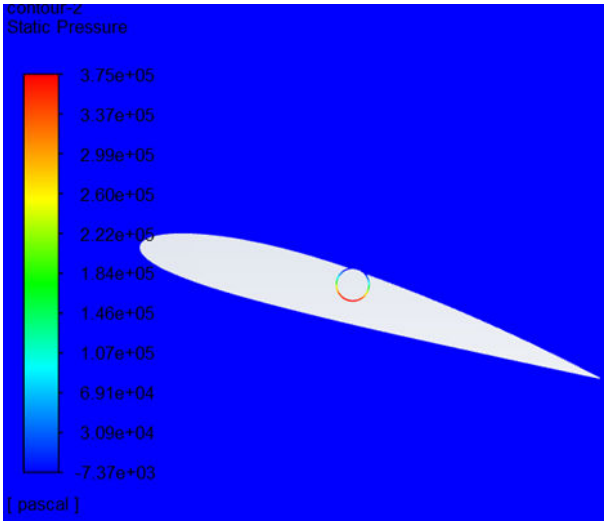

(f)

Figure 33: Pressure contour; (a) At 0°. (b) At 4°. (c) At 8°. (d) At 12°. (e) At 16°. (f) At 20°

• Velocity contour of 0.45c configuration

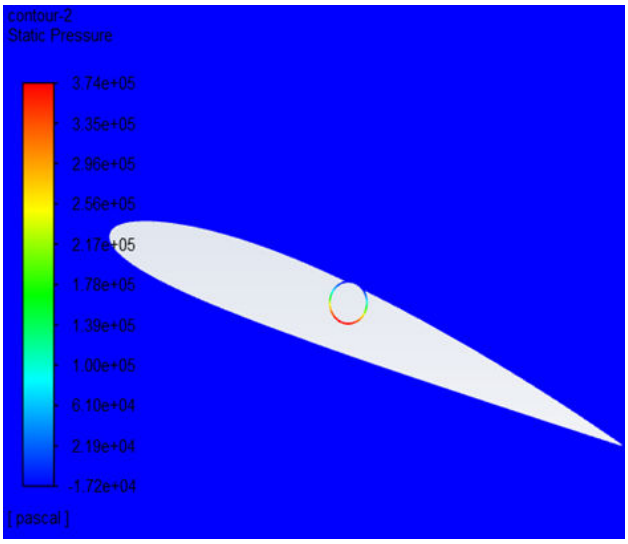

(a)

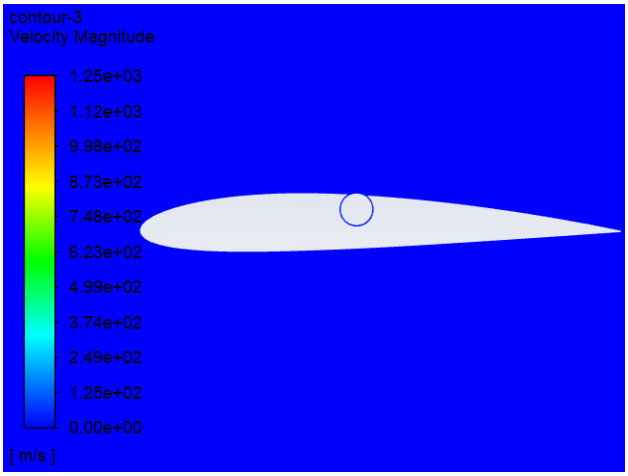

(b)

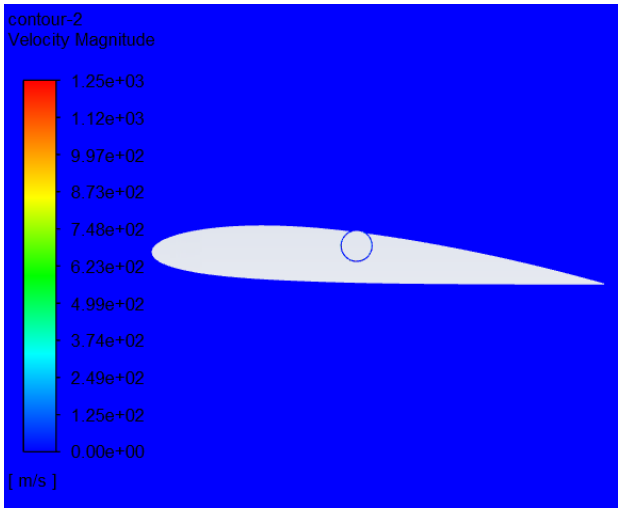

(c)

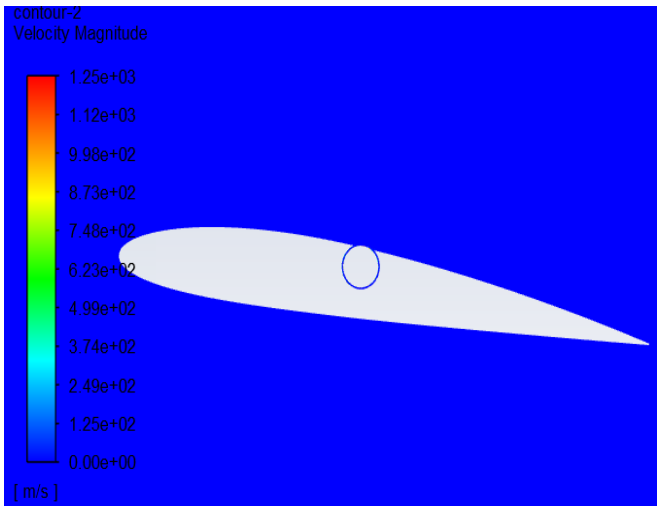

(d)

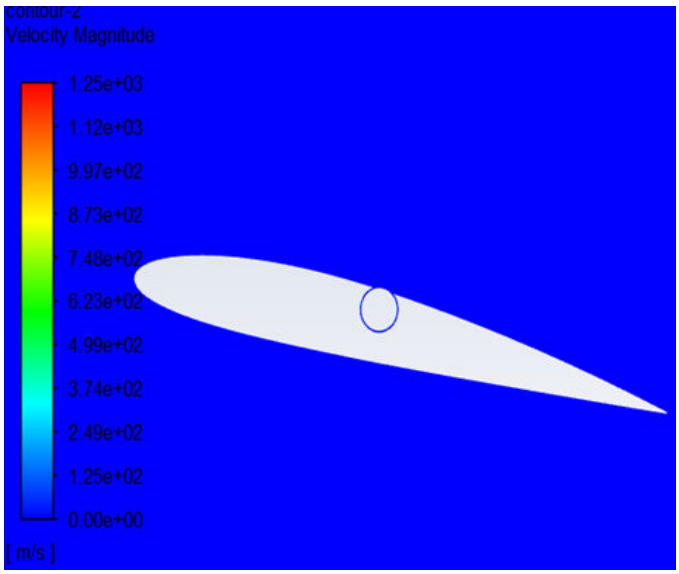

(e)

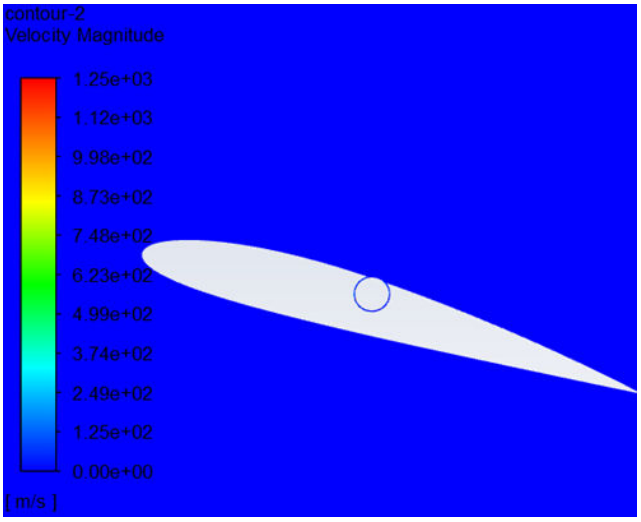

(f)

Figure 34: Velocity contour; (a) At 0°. (b) At 4°. (c) At 8°. (d) At 12°. (e) At 16°. (f) At 20°.

Velocity vector

Below (Fig 35) is the velocity vector for 0.15c configuration at 4-degree angle of attack where it can be clearly observed that the direction of flow is in clock wise direction. This applies for both 0.3c and 0.45c as well.

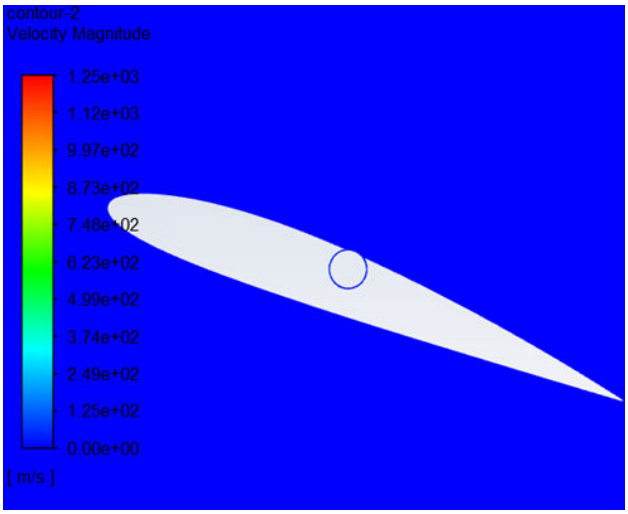

(a)

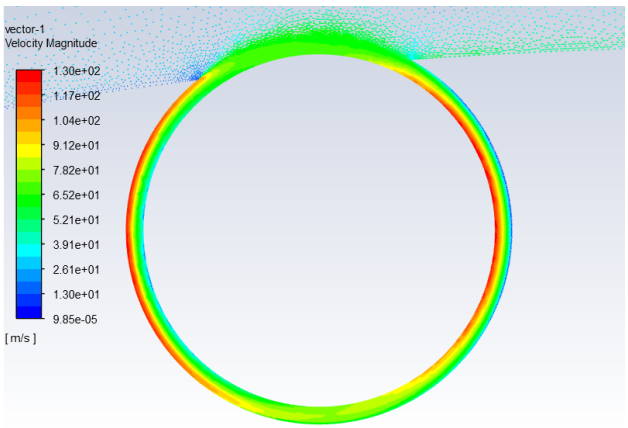

(b)

Figure 35: Velocity vector; (a) 0.15c at 4°. (b) Around the cylinder (clockwise direction).

CONCLUSION

The potential application of this will be during take-off conditions wherein a higher lift is required; this demands the aircraft to fly at a high angle of attack without stalling. Usage of a rotating cylinder as a high lift device can solve this problem. During the cruise condition, the rotating cylinder can be covered by the contour devices. This can also be used to improve flow quality as well as Stall control device that enables the aircraft to fly at higher AoA.

Looking at the outcome given by this experiment we have detected that the airfoil with the cylinder position at 0.30c at -25000 RPM, demonstrated to give better aerodynamic efficiency under comparison with other modified airfoils. It is observed that all the modified airfoils showed greater lift coefficient than bare airfoil.

However, the coefficient of drag was not as expected as it was very high when compared to bare airfoil. All these configurations cannot be used as high lift devices unless a way to deal with high drag is determined.

This project can further be enhanced by fusing blades on the cylinder and changing the blade thickness or employing forward or backward blades instead of radial. The cylinder roughness can be increased which creates friction and might make the flow stick to the surface. The cylinder can be made hollow or use diverse materials. The cylinder RPM can also be a parameter that can be considered further in similar projects.

REFRENCES

1. Dhamendra P, Abhinav Verma, Chandana J P Reddy, Jitvan Suri S, Vishal M, "Boundary layer control of airfoil using rotating cylinder", International Journal of Recent Technology and Engineering (IJRTE) ISSN:2277-3878, Volume- VIII, Issue-VI, 2020.
2. M Lopes, D. Welsh, R. Gates, J. Hoover, Mr. Lester, "The Effects of a Leading Edge Rotating Cylinder on the Performance of a NACA 0015 Airfoil at High Angles of Attack", AIAA-2014-0540, AIAA SciTech, AIAA Atmospheric Flight Mechanics Conference, 2014.
3. Er. Shivam Saxena, Mr. Rahul Kumar, "Design of NACA 2412 and its analysis at different Angle of Attacks, Reynolds Numbers and a wind tunnel".
4. Md. Abdus Salam, Bhuiyan Shameem Mahmood Ebna Hai, M. A. Taher Ali ,Debanan Bhadra , and Nafiz Ahmed Khan, "Moving surface boundary layer control analysis and the influence of the Magnus effect on an aerofoil with a leading-edge rotating cylinder", 2019.
5. Patryk Sokołowski , Jacek Czarnigowski , Paweł Magryta, "CFD simulation study of air flow around the airfoil using the magnus effect".

6. Modi, V. J. Mokhtarian, F. Effect of moving surfaces on the aerofoils boundary-layer control, Journal of Aircraft, AIAA, 1988, vol. 27(1), pp. 42–50.
7. Sahu, R., Patnaik, B.S.V. CFD simulation of momentum injection control past a streamlined body, International Journal of Numerical Methods for Heat & Fluid Flow, 2011, vol. 21(8), pp. 980–1001.
8. Buerge, B. T. The vortex flap: an experimental investigation into the use of external rotating cylinders for lift augmentation, In Proceedings of inter-national powered lift conference, London, 2009.
9. Ahmed Z. Al-Ghani, Abdullah M. Al-Garni, Saad A. Ahmed, Ahmet Z. Sahin. Flow control for an Airfoil with leading edge Rotation: An Experimental Study.
10. Dr.John E Matsson, John A. Voth, Mr. Connor A. McCain, Mr. Connor McGraw. Aerodynamic Performance of the NACA 2412 Airfoil at Low Reynolds Number.
11. F Finaish, R. Jefferies. Influence of a Rotating Leading edge on Accelerating Starting Flow over an Airfoil.
12. Control of Flow past an Airfoil section using Rotating Cylinder, ArginNazar.
13. NajdatNashad Abdulla, Mustafa Falih Hasan. Effect of Gap between Airfoil and Embedded Rotating Cylinder on the Airfoil Aerodynamic Performance.
14. Abhishek Sharma, Tejas Mishra, Sonia Chalia, Manish K. Bharti. Subsonic Flow study and analysis on Rotating cylinder Airfoil.